

# Geophysical Research Letters

## RESEARCH LETTER

10.1029/2019GL083798

### Key Points:

- The GHGSat-D satellite instrument with 50-m resolution discovered very large methane point sources from oil/gas production in Central Asia
- These large emissions were confirmed by the TROPOMI satellite instrument and extended over at least a year
- Persistently large emissions from a gas compressor station ( $10\text{--}43 \text{ t hr}^{-1}$  in >50% of observations) were observed over an 11-month period

### Supporting Information:

- Supporting Information S1

### Correspondence to:

D. J. Varon,  
danielvaron@g.harvard.edu

### Citation:

Varon, D. J., McKeever, J., Jervis, D., Maasakkers, J. D., Pandey, S., Houweling, S., et al. (2019). Satellite discovery of anomalously large methane point sources from oil/gas production. *Geophysical Research Letters*, 46. <https://doi.org/10.1029/2019GL083798>

Received 20 MAY 2019

Accepted 22 OCT 2019

Accepted article online 25 OCT 2019

## Satellite Discovery of Anomalously Large Methane Point Sources From Oil/Gas Production

D. J. Varon<sup>1,2</sup> , J. McKeever<sup>2</sup>, D. Jervis<sup>2</sup>, J. D. Maasakkers<sup>3</sup>, S. Pandey<sup>3</sup> , S. Houweling<sup>3,4</sup> , I. Aben<sup>3</sup> , T. Scarpetti<sup>5</sup>, and D. J. Jacob<sup>1</sup>

<sup>1</sup>School of Engineering and Applied Sciences, Harvard University, Cambridge, MA, USA, <sup>2</sup>GHGSat, Inc., Montréal, Quebec, Canada, <sup>3</sup>SRON Netherlands Institute for Space Research, Utrecht, Netherlands, <sup>4</sup>Department of Earth Sciences, Vrije Universiteit Amsterdam, Amsterdam, Netherlands, <sup>5</sup>Department of Earth and Planetary Sciences, Harvard University, Cambridge, MA, USA

**Abstract** Rapid identification of anomalous methane sources in oil/gas fields could enable corrective action to fight climate change. The GHGSat-D satellite instrument measuring atmospheric methane with 50-meter spatial resolution was launched in 2016 to demonstrate space-based monitoring of methane point sources. Here we report the GHGSat-D discovery of an anomalously large, persistent methane source ( $10\text{--}43$  metric tons per hour, detected in over 50% of observations) at a gas compressor station in Central Asia, together with additional sources (4–32 metric tons per hour) nearby. The TROPOMI satellite instrument confirms the magnitude of these large emissions going back to at least November 2017. We estimate that these sources released  $142 \pm 34$  metric kilotons of methane to the atmosphere from February 2018 through January 2019, comparable to the 4-month total emission from the well-documented Aliso Canyon blowout.

**Plain Language Summary** Methane is a potent greenhouse gas that is emitted from a variety of natural processes and human activities. Reducing methane emissions from oil/gas production and transmission facilities is considered to be one of the most immediately actionable ways to abate climate change, because the captured methane can be sold. Studies of U.S. oil/gas fields have shown that a small number of high-emitting facilities are responsible for the bulk of the total emission from oil/gas operations. So far, the only way to identify and quantify these sources has been through field studies involving aircraft and ground-based observations, but these are expensive, and much of the world cannot be observed in this way. Here we use satellite instruments to identify and quantify anomalously large point sources from an oil/gas field in Central Asia. Our work shows how satellite instruments can be used to monitor methane emissions from individual point sources across the world. It points to an observing strategy where instruments with global coverage at coarse spatial resolution can first identify methane hot spots and then instruments with fine spatial resolution but limited coverage can zoom in to identify the facilities responsible for the hot spots.

## 1. Introduction

Anthropogenic methane emissions originate from a large number of point sources, including coal mines, landfills, wastewater plants, livestock operations, and oil/gas facilities (Kirschke et al., 2013; Saunois et al., 2016). Methane generates 84 times more greenhouse gas warming per unit mass than carbon dioxide on a 20-year time horizon (International Panel on Climate Change, 2013). Over that time horizon, the radiative forcing of methane emitted from oil/gas operations is comparable to the radiative forcing of carbon dioxide emitted from natural gas usage (Alvarez et al., 2018). Much of the methane emitted from the oil/gas industry can be reduced or eliminated at no net cost, suggesting that reducing methane emissions from oil/gas operations is one of the most actionable steps to abate climate change (International Energy Agency, 2017).

There has been considerable interest in using satellite observations of atmospheric methane to detect and quantify methane sources, but observations available so far have only been able to resolve regional scales (~50 km), over which hundreds of individual point sources may be aggregated (Buchwitz et al., 2017; Frankenberg et al., 2005; Kort et al., 2014; Lyon et al., 2015; Turner et al., 2015). Rapid satellite-based identification of anomalously large methane sources in oil/gas fields could enable corrective action, but

©2019. The Authors.

This is an open access article under the terms of the Creative Commons Attribution License, which permits use, distribution and reproduction in any medium, provided the original work is properly cited.

subkilometer pixel resolution is needed to pinpoint individual methane-emitting facilities (Cusworth et al., 2018; Jacob et al., 2016).

Here we present single-pass satellite observations of massive methane plumes from oil/gas production and transmission infrastructure. The observations were made with the GHGSat-D and TROPOMI satellite instruments over the Korpezhe oil/gas field in western Turkmenistan. Both instruments detected large point sources in the area on multiple overpasses between November 2017 and January 2019. We use two source rate retrieval techniques to quantify emissions from the individual plume observations and estimate total emissions over the observation period from the resulting time series of emissions. Our estimates are comparable to the 4-month total emission from the 2015 blowout at the Aliso Canyon natural gas storage facility in California, which was the largest methane leak in U.S. history (Conley et al., 2016; Thompson et al., 2016). These results suggest that extreme point source methane emissions from global oil/gas operations may be much larger than previously inferred for the United States (Lyon et al., 2015; Zavala-Araiza et al., 2015) and demonstrate the potential for satellite instruments to guide efforts to reduce methane emissions from the oil/gas sector.

## 2. GHGSat-D Observations

GHGSat-D is a lightweight satellite instrument (~15-kg spacecraft) that was launched into polar sun-synchronous orbit in June 2016 by the Indian Space Research Organization. The satellite is operated by the Canadian company GHGSat Inc., which seeks to demonstrate a global capability for detecting methane emissions at the facility scale from space. GHGSat-D measures atmospheric methane columns by solar backscatter in the shortwave infrared (SWIR) over the spectral range 1,630–1,675 nm, with an effective pixel resolution of  $50 \times 50 \text{ m}^2$  over targeted  $12 \times 12 \text{ km}^2$  scenes (McKeever et al., 2017; Sloan et al., 2016; see supporting information Text S1). The measurements are made at about 10:00 local solar time, and the average return time is 2 weeks.

While targeting a mud volcano in the Balkan province of western Turkmenistan, GHGSat-D discovered on 13 January 2019 an anomalously large methane plume near the edge of its measurement domain, seemingly from a gas pipeline between the nearby Korpezhe gas production unit and compressor station, about 2 km from each facility. Another large plume originating from a piece of equipment near the compressor station was also seen on this day. Reviewing the GHGSat-D record for the scene going back to the first observation in February 2018, we found evidence of anomalously large methane plumes from three point sources corresponding to the compressor station, the connecting pipeline, and a smaller production facility about 7 km to the north. The plumes were observed in seven out of 13 clear-sky GHGSat-D observations made through the end of January 2019. The plume from the compressor station was repeatedly detected, while the plumes from the pipeline and the northern production facility were detected only once.

Figure 1 shows GHGSat-D detections of the three point sources overlaid on 2017 DigitalGlobe surface imagery of the Korpezhe oil/gas field. The most persistent source (source #1), located about 400 m southwest of the Korpezhe compressor station, appears in all seven GHGSat-D observations with detected plumes. The pipeline plume discovered on 13 January 2019 (source #2) extended more than 3 km downwind of the source location, as did the plume from source #1 on that day. The weakest source (source #3), at the northern production facility, was detected on 27 January 2019. The column density precision in these GHGSat-D observations is estimated from the variability of background columns to be 16% (see Text S1). The plumes have peak enhancements of 25–175% above background. Plume enhancement magnitudes differ from scene to scene, which may reflect variations in source magnitude as well as in atmospheric transport (Varon et al., 2018). Large temporal fluctuations in methane emissions from oil/gas point sources have previously been observed with in situ measurements in the Barnett Shale region of northeast Texas (Lyon et al., 2015) and by airborne remote sensing in the Four Corners region of New Mexico (Frankenberg et al., 2016).

It is unclear what specific activities are responsible for these large plumes. Figure 2 shows 2011–2017 DigitalGlobe imagery of the three source locations. Source #1 may be the result of venting from the compressor station. Active fire data from the Visible Infrared Imaging Radiometer Suite (Schroeder et al., 2014) available since 2012 show no burning at the source location, suggesting that it is not a flare. Source #2 appears near a pipeline connection between the Korpezhe compressor station and gas production unit. DigitalGlobe imagery from 2004 (Figure S1) shows the pipeline connection near source #2 under

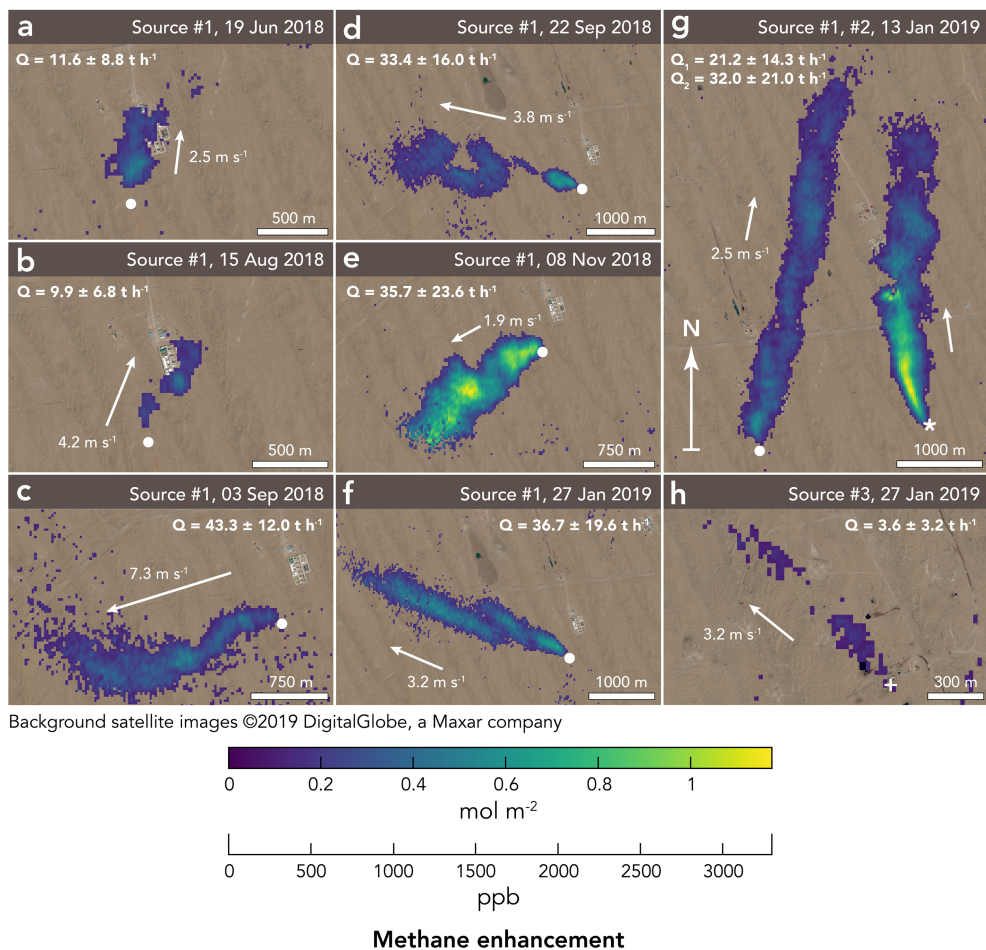
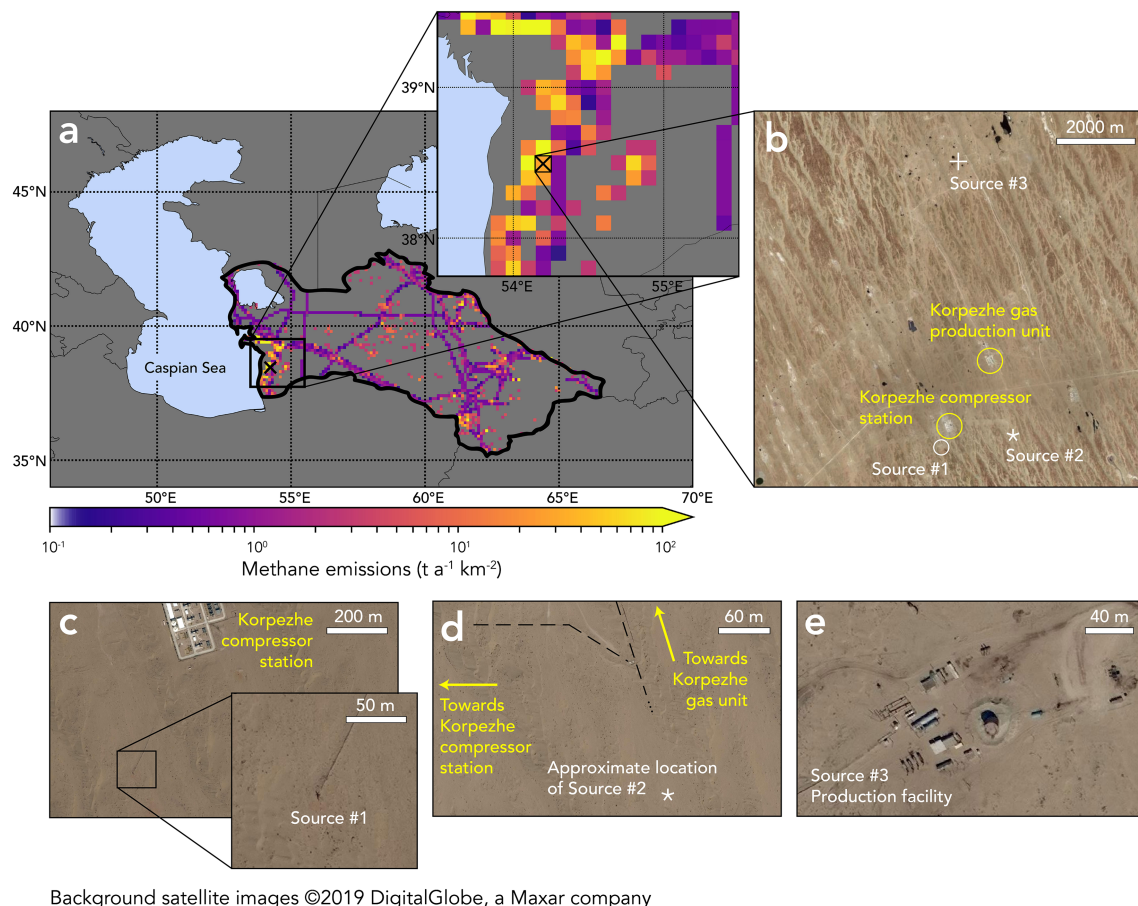


**Figure 1.** GHGSat-D observations of methane plumes in the Korpelzhe oil/gas field of western Turkmenistan. (a–h) Plumes observed near the Korpelzhe gas compressor station ( $38.499^{\circ}\text{N}$ ,  $54.199^{\circ}\text{E}$ , at sea level) between 24 February 2018 and 27 January 2019, with first detection on 19 June 2018. Methane enhancements relative to background for the scene are plotted as retrieved column enhancements ( $\text{mol m}^{-2}$ ) and converted (for illustrative purposes only) to column-averaged mixing ratios (ppb) based on sea level pressure. The plumes shown here have been segmented by thresholding at the 95th percentile, as discussed in Text S3. DigitalGlobe background imagery showing the compressor station and its surroundings is from 2017. The white disk, star, and cross symbols mark the locations of (a–g) source #1, (g) source #2, and (h) source #3, respectively (also see Figure 2). The wind vectors show the GEOS-FP 10-m wind speeds for the observations paired with the wind directions estimated from the plume enhancements and used in the cross-sectional flux method to retrieve source rates. The large plume shown in panel (e) is truncated by the edge of the GHGSat domain.

construction. A pipeline rupture would produce persistent emissions, but this is not the case here. Instead, blowdown or malfunction of an isolation valve on the pipeline branch may have produced the large emissions seen on 13 January 2019. Source #3 is a production facility. Numerous pieces of equipment could be responsible for the emissions detected from this facility on 27 January 2019.

### 3. TROPOMI Observations

Previous methane observations made in 2004 by the SCIAMACHY satellite instrument with  $60 \times 30 \text{ km}^2$  nadir pixel resolution showed a general enhancement of methane across Turkmenistan (Buchwitz et al., 2017). Here we use methane observations from the TROPOMI satellite instrument launched in October 2017 to place the GHGSat-D plume observations in context. TROPOMI is in polar sun-synchronous orbit and provides global mapping of atmospheric methane columns on daily overpasses at about 13:00 local solar time with  $7 \times 7 \text{ km}^2$  nadir pixel resolution (Hu et al., 2018; Veefkind et al., 2012). Its average  $X_{\text{CH}_4}$  bias relative to reference ground-based column measurements from Total Carbon Column Observing Network (Wunch et al., 2011) stations is  $-4.3 \text{ ppb}$ , with a station-to-station variability of  $7.4 \text{ ppb}$  (Hasekamp et al., 2019).



Background satellite images ©2019 DigitalGlobe, a Maxar company

**Figure 2.** Methane emissions inventory data and surface imagery for the GHGSat scene. (a) Methane emissions from oil/gas production, refining, processing, transport, and storage across Turkmenistan, as estimated from a global inventory with  $0.1^\circ \times 0.1^\circ$  grid resolution by Scarpelli et al. (2019). The thick line shows the boundaries of Turkmenistan. The panel inset shows a closer view of the area around Korpezhe, with the inventory grid cell containing the compressor station marked by a black “x.” (b) DigitalGlobe imagery from 2011 to 2013 showing part of the GHGSat-D scene containing sources #1–#3. Also shown are close-up views of (c) source #1, which may be a vent at the end of an aboveground pipe extending about 400 m southwest of the Korpezhe compressor station ( $38.499^\circ\text{N}$ ,  $54.199^\circ\text{E}$ ); (d) source #2, between the Korpezhe compressor station and gas production unit ( $38.514^\circ\text{N}$ ,  $54.212^\circ\text{E}$ ), with dashed lines indicating the connecting pipeline based on DigitalGlobe imagery of the pipeline under construction in 2004 (Figure S1); and (e) source #3 at the northern production facility ( $38.560^\circ\text{N}$ ,  $54.203^\circ\text{E}$ ). DigitalGlobe surface imagery in panels (c)–(e) is from 2017.

Inspection of TROPOMI data for the GHGSat-D scene over Korpezhe confirms the presence of anomalously large and persistent methane sources (Figure 3). TROPOMI first detected the sources on 16 November 2017, a few days after the instrument was switched on. Between 17 December 2017 and 31 January 2019, TROPOMI retrieved 128 successful cloud-free methane images over the Korpezhe region in which more than one pixel coincides with the GHGSat-D scene. Of these scenes, 24 were deemed suitable for emission quantification, based on the regularity of wind fields over the region (see Text S2). Plumes could often be detected up to 30 km downwind and with peak enhancements of up to 9% above background. The longer extent of the TROPOMI plumes as compared to GHGSat-D plumes reflects TROPOMI’s higher instrument precision, and the weaker enhancements reflect dilution over its larger pixels. In total, GHGSat-D and TROPOMI detected anomalously large methane emissions near the Korpezhe gas facilities respectively in 54% and over 90% of observations made between 17 December 2017 and 31 January 2019.

#### 4. Source Rate Quantification Methods

We estimate the source rate for individual plumes using two alternative methods: the integrated mass enhancement or IME (Frankenberg et al., 2016; Jongaramrungruang et al., 2019; Varon et al., 2018) and the cross-sectional flux (White et al., 1976). These methods combine the observed plume column

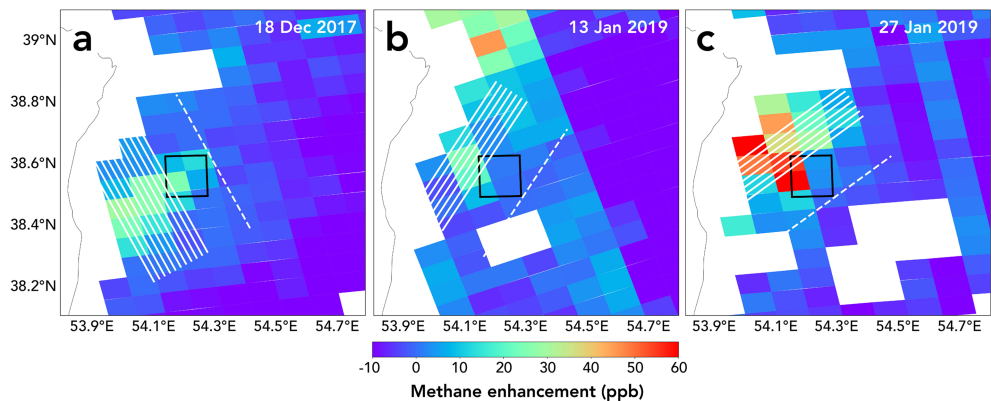


**Figure 3.** Sample TROPOMI observations of methane plumes in the Korpezhe oil/gas field. (a–c) TROPOMI methane measurements (level 2 product version 1.3.2) over the Korpezhe region on 18 December 2017, 13 January 2019, and 27 January 2019. The scenes from 13 and 27 January were selected for their concurrence with GHGSat-D observations (Figure 1). The GHGSat-D  $12 \times 12 \text{ km}^2$  domain is marked in each panel by a black square. The data represent the enhancement of methane column-averaged mixing ratio above background, where the background value is determined upwind of the GHGSat-D domain, along the dashed white line. Source strength is calculated from column concentrations along the white downwind transects, resulting in source rates of 33 (range 11–55)  $\text{t hr}^{-1}$ , 33 (6–60)  $\text{t hr}^{-1}$ , and 96 (73–124)  $\text{t hr}^{-1}$  for panels (a)–(c), respectively.

enhancements with wind speed data to infer source rate. Varon et al. (2018) give a detailed analysis of these methods as applied to satellite observations of atmospheric methane columns.

The IME method relates the source rate  $Q [\text{mol s}^{-1}]$  to the total detected plume mass IME [mol]. It uses the plume enhancements  $\Delta\Omega_i [\text{mol m}^{-2}]$  observed over  $i = 1, \dots, N$  plume pixels with area  $A_i [\text{m}^2]$ , an effective wind speed  $U_{\text{eff}} [\text{m s}^{-1}]$ , and a plume length scale  $L [\text{m}]$  to estimate  $Q$ :

$$Q = \frac{U_{\text{eff}}}{L} \text{IME} = \frac{U_{\text{eff}}}{L} \sum_{i=1}^N \Delta\Omega_i A_i. \quad (1)$$

Here  $N$  is obtained with a Boolean plume mask (see Text S3) that distinguishes plume pixels from background pixels and  $L$  is defined as the square root of the total plume area  $\sum_{i=1}^N A_i$ . Varon et al. (2018) showed with an ensemble of large eddy simulations (LES) that  $U_{\text{eff}}$  can be related to the local 10-m wind speed  $U_{10}$  in a manner that depends on the instrument precision and on the procedure used to construct the plume mask, and we apply the same methodology here. The LES ensemble comprises 15 dry air plume simulations over flat terrain, with a range of initial wind speeds and boundary layer depths. We sample the simulations at different points in time to generate a data set of GHGSat pseudo-observations, which can be used to calibrate source rate retrieval equations customized to specific measurement conditions. Applying the LES ensemble to our GHGSat-D conditions (column density precision of 16%, plume mask constructed as described in Text S3), we find  $U_{\text{eff}} = \log(U_{10}) + 0.5 \text{ m s}^{-1}$  (Figure S2).

The cross-sectional flux method infers source rate  $Q$  from column plume transects computed at different distances downwind of the source and perpendicular to the wind direction. Rotating the methane enhancements  $\Delta\Omega(x, y) [\text{mol m}^{-2}]$  to align the plume with the  $x$  axis, we estimate  $Q$  from the mean plume transect  $\bar{C} [\text{mol m}^{-1}]$  computed along the  $y$  axis at downwind distances  $x_j, j = 1, \dots, M$ :

$$Q = \bar{C} U_{\text{eff}} = \frac{U_{\text{eff}}}{M} \sum_{j=1}^M \int \Delta\Omega(x_j, y) dy. \quad (2)$$

For GHGSat-D plumes, we estimate wind direction from the shape of the plume (Figure 1), using a weighted mean of pixel coordinates with the column enhancements as weights. For TROPOMI plumes, we use wind direction information from the NASA Goddard Earth Observing System-Fast Processing (GEOS-FP) meteorological reanalysis product at  $0.25^\circ \times 0.3125^\circ$  resolution (Molod et al., 2012). The limits of the cross-plume integral in equation (2) are defined by transects of fixed length for TROPOMI plumes (Figure 3) and by

the Boolean plume mask constructed in the IME method for GHGSat-D plumes. The effective wind speed  $U_{\text{eff}}$  in equation (2) is different than for the IME method but can again be related to the local 10-m wind speed  $U_{10}$  using our LES ensemble. We obtain  $U_{\text{eff}} = 1.5U_{10}$  (Figure S2).

For GHGSat-D plumes, we apply both the cross-sectional flux and IME methods as independent inferences of source rate, using hourly  $U_{10}$  data from GEOS-FP to estimate  $U_{\text{eff}}$ . Source rates obtained with the IME and cross-sectional flux methods agree to within 50% for single-pass observations (Figure S3), so we report the average of the two estimates for each plume (Figure 1 and Table S1). Since the cross-sectional flux method can be unreliable for  $U_{10} < 2 \text{ m s}^{-1}$  (Varon et al., 2018), we use only the IME method for the plume observed under low wind conditions on 8 November 2018 (Figure 1e). The source rate on this day may be underestimated due to the plume's truncation at the edge of the measurement domain. Errors on the source rates (Table S1) are estimated following Varon et al. (2018) and are dominated by uncertainty in  $U_{10}$ . By comparing GEOS-FP  $U_{10}$  data with 5-min observations from U.S. airports (Horel et al., 2002), Varon et al. (2018) estimated an error of ( $1\sigma$ )  $2\text{--}2.5 \text{ m s}^{-1}$  when using GEOS-FP to estimate  $U_{10}$ , and we assume that the same error applies here. GEOS-FP 10-m wind speeds for our GHGSat-D scenes range from  $1.9$  to  $7.3 \text{ m s}^{-1}$  (Figure 1), and the total errors in source rate range from 30% to 90% (larger error for low winds; see Table S1 and Text S4). Relative source rate errors under low wind speed conditions are smaller than would be expected from  $U_{10}$  uncertainty of  $2\text{--}2.5 \text{ m s}^{-1}$ , because relative errors in  $U_{\text{eff}}$  are generally smaller than those in  $U_{10}$ . This is due to the convexity of the effective wind speed function used in the IME method (see Figure S2), which reduces variance in effective wind speed, and also more generally to wind speed being strictly positive, which reduces absolute error variance for slow compared to fast winds.

For plumes detected by TROPOMI, we use the cross-sectional flux method with pressure-weighted average planetary boundary layer winds  $U_{\text{BL}}$  from GEOS-FP instead of  $U_{10}$ , and estimate errors on source rate from an ensemble of retrievals using different meteorological information, plume sampling, and background estimation schemes (see Text S5). The quantification assumes a source confined to the GHGSat-D spatial domain and is performed with transects of length  $0.5^\circ$ , separated by  $0.02^\circ$  along the plume axis (Figure 3). We characterize the relationship between  $U_{\text{eff}}$  and  $U_{\text{BL}}$  using the Weather Research and Forecasting model coupled with chemistry (WRF-Chem version 3.8.1; Grell & Freitas, 2014; Skamarock et al., 2008). WRF-Chem simulations of methane concentrations were performed at 1-km horizontal resolution over Korpezhe for all quantifiable plumes in January 2019 (13, 16, 24, and 27 January 2019), using analysis meteorological fields from National Centers for Environmental Prediction (2000). We modeled emissions for sources #1–#3 using mean source rates inferred from the GHGSat-D observations and virtually sampled the resulting simulated methane fields with TROPOMI at 9:00 UTC (about 13:00 local solar time). Applying the cross-sectional flux method to these simulated observations, we estimate the relationship between  $U_{\text{eff}}$  and  $U_{\text{BL}}$  by comparing the resulting source rates to the simulation ground truths. We find on average that  $U_{\text{eff}} = (1.05 \pm 0.17)U_{\text{BL}}$ . We then use this relationship to infer source rates from all of our TROPOMI observations (except those from January 2019, for which we use the specific  $U_{\text{eff}}\text{--}U_{\text{BL}}$  relationships derived from the corresponding simulations). Figure 4 shows the results, with vertical bars giving the ranges for the ensemble of retrievals. We take the half-length of these vertical bars to represent the uncertainty, amounting on average to 60% of the best estimate of the source rate. Source rates for the 24 quantified scenes are converted to a time-averaged source rate after correcting for representativeness by comparing the mean peak enhancement for these 24 scenes with the mean peak enhancement for the 128 scenes over the full observation record (see Text S2).

## 5. Source Rate Estimates

From retrieval of source rates for the individual GHGSat-D plumes, we infer instantaneous values of  $9.9 \pm 6.8$  to  $43.3 \pm 12.0 \text{ t hr}^{-1}$  for the compressor station source (source #1),  $32.0 \pm 21.0 \text{ t hr}^{-1}$  for the pipeline source (source #2), and  $3.6 \pm 3.2 \text{ t hr}^{-1}$  for the northern facility (source #3). These rates are considerably larger than the  $0.3\text{--}2.0 \text{ t hr}^{-1}$  previously reported for anomalous (heavy-tail) point sources from oil/gas production in the United States (Lyon et al., 2015), including typical compressor station blowdown emissions of  $\sim 0.25 \text{ t hr}^{-1}$  (United States Environmental Protection Agency, 2006). They are comparable to emissions from major oil/gas accidents like the well-publicized 2015 Aliso Canyon (peak rate of  $60 \text{ t hr}^{-1}$ ; Conley et al., 2016;

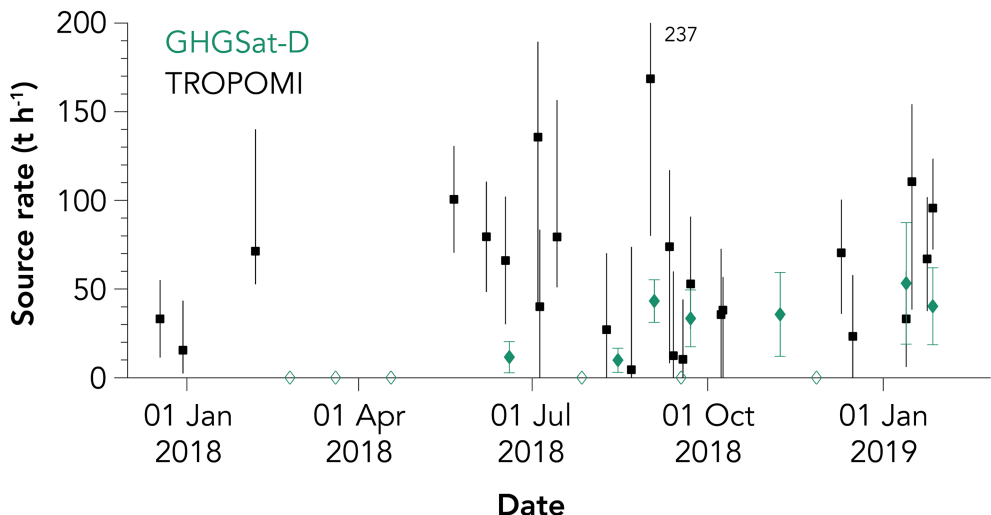


**Figure 4.** Time series of emissions from the Korpezhe  $12 \times 12 \text{ km}^2$  scene. Source rates inferred from GHGSat-D observations (green diamonds) include emissions from all plumes detected across the scene. Source rates inferred from TROPOMI observations (black squares) may include additional plumes within the scene and downwind. The GHGSat-D observation record is from 24 February 2018 to 27 January 2019, and the TROPOMI observation record is from 17 December 2017 to 31 January 2019. The green error bars represent error standard deviations ( $1\sigma$ ) on the source rates inferred from GHGSat-D observations. The black vertical bars represent the range of emissions inferred from the TROPOMI source rate retrieval ensemble for each quantified plume. Green open markers denote GHGSat-D scenes where no plumes were detected. TROPOMI source rates are from observations with quantifiable plumes; many TROPOMI detection events are not shown here due to ambiguity in meteorology for inferring source rates.

Thompson et al., 2016) and 2018 Ohio well pad (peak rate  $>75 \text{ t hr}^{-1}$ ; Pandey et al., 2018; United States Environmental Protection Agency, 2018) blowouts.

Figure 4 shows the December 2017 to January 2019 time series of source rates estimated by GHGSat-D and TROPOMI for the  $12 \times 12 \text{ km}^2$  GHGSat-D scene. Source rates for GHGSat-D observations with multiple plumes are given as the total emissions for all plumes in the scene. This results in scene-wide emissions of  $9.9 \pm 6.8$  to  $53.2 \pm 34.3 \text{ t hr}^{-1}$  for observations with detected plumes, for a mean of  $32.5 \pm 7.7 \text{ t hr}^{-1}$  when plumes are present and  $17.5 \pm 4.2 \text{ t hr}^{-1}$  when including plume-free observations in the average. The uncertainties on these mean hourly rates are derived by propagating source rate error standard deviations from individual days (Figure 1 and Table S1) through the calculation of the mean (see Text S4). The range of source rates across all quantified TROPOMI observations is  $5\text{--}169 \text{ t hr}^{-1}$ , with a mean of  $60 \text{ t hr}^{-1}$  for quantifiable plumes and  $45 \text{ t hr}^{-1}$  over the full observation record. TROPOMI source rate estimates tend to be larger than those from GHGSat-D, possibly due to additional sources downwind of the GHGSat-D scene that would be incorporated into the broader TROPOMI plumes. In addition, GHGSat-D would miss point sources emitting below its detection threshold. Discrepancies in the source rate estimated with GHGSat-D and TROPOMI on days with concurrent measurements (e.g., 13 and 27 January 2019) may be partly attributable to these signal differences, but also to source rate retrieval error and temporal variability of emissions during the roughly 3-hr window between instrument overpasses.

If our ensemble of GHGSat-D and TROPOMI observations is representative of emissions from the Korpezhe  $12 \times 12 \text{ km}^2$  scene over the instruments' observation periods, we estimate total methane emissions of  $142 \pm 34 \text{ kt}$  from the three sources detected by GHGSat-D between 24 February 2018 and 27 January 2019 ( $\approx 153 \pm 37 \text{ kt a}^{-1}$ ) and  $446$  ( $189\text{--}750$ ) kt for the ensemble of sources detected by TROPOMI between 17 December 2017 and 31 January 2019 ( $\approx 396$  [ $168\text{--}666$ ] kt a $^{-1}$ ). Estimated emissions from the Korpezhe compressor station source alone are  $120 \pm 27 \text{ kt}$  for the February 2018 to January 2019 period ( $\approx 129 \pm 29 \text{ kt a}^{-1}$ ) according to GHGSat-D. For comparison, the 2015 Aliso Canyon blowout emitted  $97 \text{ kt}$  of methane to the atmosphere over a 4-month period (Conley et al., 2016), and the largest reported methane point sources in the United States (coal mines and landfills) emit  $10\text{--}100 \text{ kt a}^{-1}$  (Jacob et al., 2016). Our estimates of total and annual emissions from the Korpezhe sources are calculated by multiplying average retrieved source rates by duration (e.g., 1 year), with all observations counted in the average (including nondetections, for which

we assume zero emissions). The assumption of representative sampling is more reliable for TROPOMI than for GHGSat-D, both because the TROPOMI data set has larger sample size and because with its coarser pixels TROPOMI sees emissions integrated over longer periods of time (several hours).

## 6. Conclusions

Our discovery of anomalously large methane emissions associated with the Korpezhe gas compressor station in western Turkmenistan demonstrates the value of satellites for identifying and monitoring methane emissions at the facility scale worldwide. Anomalous point sources are known to make a disproportionately large contribution to the total methane emission from oil/gas production (Alvarez et al., 2018; Zavala-Araiza et al., 2015), and our results indicate that this contribution could be even larger than has been previously recognized. Detection of these point sources using satellite observations could enable corrective action to significantly reduce methane emissions from the oil/gas sector. GHGSat-D serves as demonstration for a future constellation of GHGSat satellite instruments to be launched starting in 2020 with improved column density precision (McKeever et al., 2017). The synergy with TROPOMI observations demonstrated here points to a promising observation strategy in which coarse identification of methane hot spots by TROPOMI can guide fine-resolution satellites like GHGSat-D to identify the specific facilities responsible for the hot spots and direct intervention accordingly.

## Data Availability Statements

The meteorological data sets that support the findings of this study are available at their respective online data portals: (GEOS-FP) gmao.gsfc.nasa.gov/GMAO\_products; (ERA) www.ecmwf.int/en/forecasts/datasets/browse-reanalysis-datasets; (NCEP) www.esrl.noaa.gov/psd/data/gridded/data.ncep.reanalysis.html; and (MesoWest) mesowest.utah.edu/. Visible Infrared Imaging Radiometer Suite data are posted online (earthdata.nasa.gov). The oil/gas infrastructure emissions data that support the findings of this study are publicly available (<https://doi.org/10.7910/DVN/HH4EUM>). The TROPOMI methane data are posted online (scihub.copernicus.eu). The GHGSat-D methane columns data that support the findings of this study are publicly available (<https://doi.org/10.7910/DVN/MAPGNU>).

## Conflict of Interests

The authors declare no competing interests.

## Acknowledgments

We thank O. B. A. Durak and J. J. Sloan for their roles in developing the GHGSat retrievals algorithm and measurement concept. We thank C. Herzog, M. Arias, and K. Wisniewski for technical assistance and preparation of the GHGSat-D methane data. We thank the team that realized the TROPOMI instrument and its data products, consisting of the partnership between Airbus Defense and Space, KNMI, SRON, and TNO, commissioned by NSO and ESA. Sentinel-5 Precursor is part of the EU Copernicus program, and Copernicus (modified) Sentinel data 2017–2019 have been used. D. J. J. was supported by the Carbon Monitoring System of the NASA Earth Science Division. S. P. is funded through the GALES project (15597) by the Dutch Technology Foundation STW, which is part of the Netherlands Organization for Scientific Research (NWO), and is partly funded by Ministry of Economic Affairs. Part of this work was carried out on the Dutch national e-infrastructure with the support of SURF Cooperative.

## References

- Alvarez, R. A., Zavala-Araiza, D., Lyon, D. R., Allen, D. T., Barkley, Z. R., Brandt, A. R., et al. (2018). Assessment of methane emissions from the U.S. oil and gas supply chain. *Science*, 361, 186–188. <https://doi.org/10.1126/science.aar7204>
- Buchwitz, M., Schneising, O., Reuter, M., Heymann, J., Krautwurst, S., Bovensmann, H., et al. (2017). Satellite-derived methane hotspot emission estimates using a fast data-driven method. *Atmospheric Chemistry and Physics*, 17(9), 5751–5774. <https://doi.org/10.5194/acp-17-5751-2017>
- Conley, S., Franco, G., Faloona, I., Blake, D. R., Peischl, J., & Ryerson, T. B. (2016). Methane emissions from the 2015 Aliso Canyon blowout in Los Angeles, CA. *Science*, 351, 1317–1320. <https://doi.org/10.1126/science.aaf2348>
- Cusworth, D. H., Jacob, D. J., Sheng, J. X., Benmergui, J., Turner, A. J., Brandman, J., et al. (2018). Detecting high-emitting methane sources in oil/gas fields using satellite observations. *Atmospheric Chemistry and Physics*, 18(23), 16,885–16,896. <https://doi.org/10.5194/acp-18-16885-2018>
- Frankenberg, C., Meirink, J. F., van Weele, M., Platt, U., & Wagner, T. (2005). Assessing methane emissions from global space-borne observations. *Science*, 308, 1010–1014. <https://doi.org/10.1126/science.1106644>
- Frankenberg, C., Thorpe, A. K., Thompson, D. R., Hulley, G., Kort, E. A., Vance, N., et al. (2016). Airborne methane remote measurements reveal heavy-tail flux distribution in Four Corners region. *Proceedings of the National Academy of Sciences of the United States of America*, 113(35), 9734–9739. <https://doi.org/10.1073/pnas.1605617113>
- Grell, G. A., & Freitas, S. R. (2014). A scale and aerosol aware stochastic convective parameterization for weather and air quality modeling. *Atmospheric Chemistry and Physics*, 14, 5233–5250. <https://doi.org/10.5194/acp-14-5233-2014>
- Hasekamp, O., Lorente, A., Hu, H., Butz, A., Aan de Brugh, J., & Landgraf, J. (2019). Algorithm Theoretical Baseline Document for Sentinel-5 Precursor Methane Retrieval (SRON-S5P-LEV2-RP-001, 2019). <https://sentinel.esa.int/documents/247904/2476257/Sentinel-5P-TROPOMI-ATBD-Methane-retrieval>
- Horel, J., Splitter, M., Dunn, L., Pechmann, J., White, B., Ciliberti, C., et al. (2002). MesoWest: Cooperative mesonets in the western United States. *Bulletin of the American Meteorological Society*, 83(2), 211–225. [https://doi.org/10.1175/15200477\(2002\)083<0211:MCMTW>2.3.CO;2](https://doi.org/10.1175/15200477(2002)083<0211:MCMTW>2.3.CO;2)
- Hu, H., Landgraf, J., Detmers, R., Borsdorff, T., aan de Brugh, J., Aben, I., et al. (2018). Toward global mapping of methane with TROPOMI: First results and intersatellite comparison to GOSAT. *Geophysical Research Letters*, 45, 3682–3689. <https://doi.org/10.1002/2018GL077259>
- International Energy Agency (2017). *World Energy Outlook 2017*. Paris: IEA, Paris: OECD Publishing. 2017

- International Panel on Climate Change (2013). *Climate change 2013: The physical science basis. Contribution of Working Group I to the Fifth Assessment Report of the Intergovernmental Panel on Climate Change*. New York: IPCC, Cambridge University Press. 2013
- Jacob, D. J., Turner, A. J., Maasakkers, J. D., Sheng, J., Sun, K., Liu, X., et al. (2016). Satellite observations of atmospheric methane and their value for quantifying methane emissions. *Atmospheric Chemistry and Physics*, 16(22), 14,371–14,396. <https://doi.org/10.5194/acp-16-14371-2016>
- Jongaramrungruang, S., Frankenberg, C., Matheou, G., Thorpe, A. K., Thompson, D. R., Kuai, L., & Duren, R. (2019). Towards accurate methane point-source quantification from high-resolution 2D plume imagery. *Atmospheric Measurement Techniques*, <https://doi.org/10.5194/amt-2019-173>.
- Kirschke, S., Bousquet, P., Ciais, P., Saunois, M., Canadell, J. G., Dlugokencky, E. J., et al. (2013). Three decades of global methane sources and sinks. *Nature Geoscience*, 6(10), 813–823. <https://doi.org/10.1038/ngeo1955>
- Kort, E. A., Frankenberg, C., Costigan, K. R., Lindenmaier, R., Dubey, M. K., & Wunch, D. (2014). Four corners: The largest U.S. methane anomaly viewed from space. *Geophysical Research Letters*, 41, 6898–6903. <https://doi.org/10.1002/2014GL061503>
- Lyon, D. R., Zavala-Araiza, D., Alvarez, R. A., Harriss, R., Palacios, V., Lan, X., et al. (2015). Constructing a spatially resolved methane emission inventory for the Barnett Shale Region. *Environmental Science & Technology*, 49(13), 8147–8157. <https://doi.org/10.1021/es506359c>
- McKeever, J., Durak, B. O. A., Gains, D., Varon, D. J., Germain, S., & Sloan, J. J. (2017). GHGSat-D: Greenhouse gas plume imaging and quantification from space using a Fabry-Perot imaging spectrometer. Abstract presented at the American Geophysical Union 2017 Fall Meeting, New Orleans, LA, 11–15 December 2017.
- Molod, A., Takacs, L., Suarez, M., Bacmeister, J., In-Sun, S., & Eichmann, A. (2012). The GEOS-5 atmospheric general circulation model: Mean climate and development from MERRA to Fortuna (Technical Report Series on Global Modeling and Data Assimilation, Volume 28, 2012).
- National Centers for Environmental Prediction (2000) updated daily. NCEP FNL operational model global tropospheric analyses, continuing from July 1999 (NCEP, 2000). <https://doi.org/10.5065/D6M043C6>
- Pandey, S., Houweling, S., Hu, H., Sadavarte, P., Gautam, R., Hasekamp, O.P., et al., (2018). Early analysis of TROPOMI X<sub>CH<sub>4</sub></sub> for detection and quantification of local CH<sub>4</sub> emissions. Paper presented at the American Geophysical Union 2018 Fall Meeting, Washington, DC, 12 December 2018.
- Saunois, M., Bousquet, P., Poulter, B., Peregon, A., Ciais, P., Canadell, J. G., et al. (2016). The global methane budget 2000–2012. *Earth System Science Data*, 8(2), 697–751. <https://doi.org/10.5194/essd-8-697-2016>
- Scarpelli, T. R., Jacob, D. J., Maasakkers, J. D., Sulprizio, M. P., Sheng, J.; Rose, K., et al. (2019). A global gridded (0.1° × 0.1°) inventory of methane emissions from oil, gas, and coal exploitation based on national reports to the United Nations Framework Convention on Climate Change, *Earth Syst. Sci. Data Discuss.*, <https://doi.org/10.5194/essd-2019-127>
- Schroeder, W., Oliva, P., Giglio, L., & Csiszar, I. A. (2014). The New VIIRS 375 m active fire detection data product: Algorithm description and initial assessment. *Remote Sensing of Environment*, 143, 85–96. <https://doi.org/10.1016/j.rse.2013.12.008>
- Skamarock, W. C., Klemp, J. B., Dudhia, J., Gill, D. O., Barker, D. M., Duda, M. G., et al., (2008). A description of the Advanced Research WRF Version 3 (Technical report, National Center for Atmospheric Research, 2008).
- Sloan, J. J., Durak, B., Gains, D., Ricci, F., McKeever, J., Lamorie, J., et al. (2016). Fabry-Perot interferometer based satellite detection of atmospheric trace gases. US 9,228,897 B2, United States Patent and Trademark Office. Retrieved from <https://patentimages.storage.googleapis.com/85/4e/65/b3f964823f2f3b/US9228897.pdf>
- Thompson, D. R., Thorpe, A. K., Frankenberg, C., Green, R. O., Duren, R., Guanter, L., et al. (2016). Space-based remote imaging spectroscopy of the Aliso Canyon CH<sub>4</sub> superemitter. *Geophysical Research Letters*, 43, 6571–6578. <https://doi.org/10.1002/2016GL069079>
- Turner, A. J., Jacob, D. J., Wecht, K. J., Maasakkers, J. D., Lundgren, E., Andrews, A. E., et al. (2015). Estimating global and North American methane emissions with high spatial resolution using GOSAT satellite data. *Atmospheric Chemistry and Physics*, 15(12), 7049–7069. <https://doi.org/10.5194/acp-15-7049-2015>
- United States Environmental Protection Agency (2006). Reducing emissions when taking compressors off-line. Available at [https://www.epa.gov/sites/production/files/2016-06/documents/l1\\_compressorsoffline.pdf](https://www.epa.gov/sites/production/files/2016-06/documents/l1_compressorsoffline.pdf)
- United States Environmental Protection Agency (2018). XTO energy well blowout—E18152—Removal Polrep—Initial Removal Polrep. (U.S. Environmental Protection Agency Pollution/Situation Report). Available at [https://www.fractracker.org/a5ej20sfwe/wp-content/uploads/2018/03/XTOPowhatenPoint\\_polrep\\_1.pdf](https://www.fractracker.org/a5ej20sfwe/wp-content/uploads/2018/03/XTOPowhatenPoint_polrep_1.pdf)
- Varon, D. J., Jacob, D. J., McKeever, J., Jervis, D., Durak, B. O. A., Xia, Y., & Huang, Y. (2018). Quantifying methane point sources from fine-scale satellite observations of atmospheric methane plumes. *Atmospheric Measurement Techniques*, 11, 5673–5686. <https://doi.org/10.5194/amt-11-5673-2018>
- Veefkind, J. P., Aben, I., McMullan, K., Förster, H., de Vries, J., Otter, G., et al. (2012). TROPOMI on the ESA Sentinel-5 Precursor: A GMES mission for global observations of the atmospheric composition for climate, air quality and ozone layer applications. *Remote Sensing of Environment*, 120, 70–83. <https://doi.org/10.1016/j.rse.2011.09.027>
- White, W. H., Anderson, J. A., Blumenthal, D. L., Husar, R. B., Gillani, N. V., Husar, J. D., & Wilson, W. E. Jr. (1976). Formation and transport of secondary air pollutants: Ozone and aerosols in the St. Louis urban plume. *Science*, 194(4261), 187–189. <https://doi.org/10.1126/science.959846>
- Wunch, D., Toon, G. C., Blavier, J. F. L., Washenfelder, R. A., Notholt, J., Connor, B. J., et al. (2011). The total carbon column observing network. *Philosophical Transactions of the Royal Society A: Mathematical, Physical and Engineering Sciences*, 369(1943), 2087–2112. <https://doi.org/10.1098/rsta.2010.0240>
- Zavala-Araiza, D., Lyon, D., Alvarez, R. A., Palacios, V., Harriss, R., Lan, X., et al. (2015). Toward a functional definition of methane super-emitters: Application to natural gas production sites. *Environmental Science & Technology*, 49(13), 8167–8174. <https://doi.org/10.1021/es500133>

## References From the Supporting Information

- Atmospheric and Environmental Research (AER) (2017). Solar irradiance spectrum extract\_solar\_v1.4.4. Retrieved from [http://rtweb.aer.com/solar\\_frame.html](http://rtweb.aer.com/solar_frame.html) (last update August 2017).
- Copernicus Climate Change Service (C3S) (2019). ERA5: Fifth generation of ECMWF atmospheric reanalyses of the global climate (Copernicus Climate Change Service Climate Data Store (CDS), 2019). <https://cds.climate.copernicus.eu/cdsapp#!/home>

- Dee, D. P., Uppala, S. M., Simmons, A. J., Berrisford, P., Poli, P., Kobayashi, S., et al. (2011). The ERA-Interim reanalysis: Configuration and performance of the data assimilation system. *Quarterly Journal of the Royal Meteorological Society*, 137(656), 553–597. <https://doi.org/10.1002/qj.828>
- Kochanov, R. V., Gordon, I. E., Rothman, L. S., Wcislo, P., Hill, C., & Wilzewski, J. S. (2016). HITRAN Application Programming Interface (HAPI): A comprehensive approach to working with spectroscopic data. *Journal of Quantitative Spectroscopy and Radiative Transfer*, 177, 15–30.
- Razavi, A., Clerbaux, C., Wespes, C., Clarisse, L., Hurtmans, D., Payan, S., et al. (2009). Characterization of methane retrievals from the IASI space-borne sounder. *Atmospheric Chemistry and Physics*, 9(20), 7889–7899. <https://doi.org/10.5194/acp-9-7889-2009>
- Rodgers, C. D. (2000). Inverse methods for atmospheric sounding: Theory and practice (Vol. 2). World scientific.
- Roy, D. P., Wulder, M. A., Loveland, T. R., Allen, R. G., Anderson, M. C., Helder, D., et al. (2014). Landsat-8: Science and product vision for terrestrial global change research. *Remote Sensing of Environment*, 145, 154–172. <https://doi.org/10.1016/j.rse.2014.02.001>
- Tobin, D. C., Revercomb, H. E., Knuteson, R. O., Lesht, B. M., Strow, L. L., Hannon, S. E., et al. (2006). Atmospheric Radiation Measurement site atmospheric state best estimates for Atmospheric Infrared Sounder temperature and water vapor retrieval validation. *Journal of Geophysical Research*, 111, D09S14. <https://doi.org/10.1029/2005JD006103>